ORIGINAL PAPER

Expansion of the planar-fit method to estimate flux over complex terrain

**Renmin Yuan · Minseok Kang · Sung-Bin Park ·
Jinkyu Hong · Dongho Lee · Joon Kim**

Abstract An expanded planar-fit (PF) method over complex terrain is presented and applied to coordinate rotation of the eddy-covariance (EC) flux and vertical velocity estimation. Theoretical analysis indicates that PF coefficients depend on wind direction, and an expression of vertical velocity is deduced. We applied the theory using 1 year of observations from the KoFlux site in the Gwangneung Forest in Korea and investigated the influence of wind direction on the PF method. Then, we performed an expansion of the PF method to consider dependence of PF coefficients on wind direction and applied the PF method to every sector. The results show that the PF coefficients and tilt angles over complex terrain vary with wind direction. Two hundred 30-min data sets are sufficient to derive stable PF coefficients over hilly terrain for each sector. The relative difference in eddy-covariance flux between the general planar fit (GPF) and sector planar fit (SPF) is less than 10% for the scalar flux and about 18% for friction velocity. Vertical velocity and vertical advection (VA) terms were also calculated and compared using SPF and GPF methods, and a normal distribution and diurnal trend of real vertical velocity on clear days are presented.

R. Yuan (✉)
School of Earth and Space Sciences, University of Science
and Technology of China, Hefei 230026, China
e-mail: rmyuan@ustc.edu.cn

R. Yuan · M. Kang · S.-B. Park · J. Hong · D. Lee · J. Kim
Department of Atmospheric Sciences, Yonsei University,
Seoul 120-749, Korea

1 Introduction

The exchange of momentum, heat and water vapor between the atmosphere and the Earth's surface has a marked effect on atmospheric motion, and the increase in atmospheric CO_2 concentration constitutes a critical change of the Earth's climate system. To investigate these phenomena, a number of international land–atmosphere flux measurement networks with eddy-covariance (EC) and multi-level profile systems have been established to monitor the carbon and water cycles in the terrestrial environment (Yu et al. 2006; Baldocchi et al. 2001). Many investigators have found that these flux measurements often do not satisfy a fundamental criterion, namely, closure of the surface energy balance (Oncley et al. 2007; Mauder et al. 2007). It is important to determine the reasons for this deficit because, otherwise, it is impossible to use experimental data to evaluate new and existing models. For example, the evaluation of sub-grid parameterizations of surface-atmosphere transfer schemes in climate numerical models is impossible because we do not know which components of the energy balance might be incorrectly estimated.

The lack of energy-balance closure may be related to three issues: the direct measurement of all terms of the energy budget using comparable scales, instrumentation and post-data-processing methods (Oncley et al. 2007). For flux measurements, the eddy-covariance method is a primary method of measuring turbulent fluxes directly, providing a high temporal resolution of spatially integrated exchange flux. This method has been considered as an important tool for evaluating fluxes of carbon dioxide and water vapor between terrestrial ecosystems and the atmosphere (Baldocchi 2003).

Generally, vector quantities such as velocities or fluxes are measured by the eddy-covariance instruments in a

reference system that does not coincide with that of the equations used to analyze them. Before the observed fluxes can be meaningfully interpreted, choosing a proper coordinate system and calculation method is a necessary step in micrometeorological studies of surface-air exchange. The most common rotation procedure uses measured mean wind to define an orthogonal-vector basis for each observational period (e.g., 30 min) for which all fluxes are transformed. The rotation scheme for determining the tilt angles for placement of the sonic anemometer into a stream-wise coordinate system (i.e., natural wind system) involves double rotations (DR) and triple rotations (TR) (Tanner and Thurtell 1969; Kaimal and Finnigan 1994; Lee et al. 2004). In the DR method, the x-axis is aligned with the mean flow, and the mean vertical velocity is zero at the end of each average period. The TR method was employed to align mean flow into mean Reynolds stress, and the new y- and z-axes are rotated around the new x-axis until the cross-stream stress becomes zero (i.e., $\overline{v'w'} = 0$). DR and TR are relatively easy to understand and apply. For homogeneous surfaces, the DR or TR attributes the mean vertical wind to the sensor tilt in leveling the sonic anemometer. Thus, they permit only one-dimensional flow; e.g., the velocity and scalar concentration gradients exist only in the vertical direction. Therefore, the horizontal scalar advection or the flow divergence does not exist, and there is no wind directional shear causing a cross-wind momentum flux. However, 2- and 3-dimensional flows, such as thermal circulation and free convection, can generate non-zero mean vertical wind speed (Lee 1998; Finnigan 1999). In this case, over-rotation results in a systematic bias in the surface-flux computation. Furthermore, the random sampling error of surface fluxes is relatively large in the DR and TR under light wind conditions because the random sampling error affects the components for the rotation method, which, in turn, will affect the errors in the fluxes (Wilczak et al. 2001). In general, scalar fluxes are not particularly sensitive to tilt bias, but momentum fluxes significantly depend on the coordinate frame (Lee et al. 2004).

The planar-fit (PF) method for tilt correction was introduced by Wilczak et al. (2001) to overcome the limitations of the DR and TR. This method utilizes a right-hand orthogonal coordinate frame using an ensemble of individual 30-min (or 15-min) records. That is, based on the measured mean wind vector during the entire experimental period, a fitted plane is obtained using multiple-linear regression. Therefore, the PF rotation can make a stable coordinate frame and minimize the over-rotation due to the flow distortion by instruments and tower frame so as to maintain information on 2- and 3-dimensional flows, such as thermal circulation and free convection. The mean vertical velocity on this plane over the long term is zero, but individual data runs have non-zero mean vertical wind.

The PF method has been used widely for coordinate rotation on the eddy-covariance flux estimation (Lee et al. 2004) and produces correct results over local terrain that follows a plane surface with small curvature. However, flux measurement sites are often found over complex terrain with large curvatures, sometimes at different slopes in different directions. It is difficult to fit one plane over such complex terrain. Therefore, the complexity of the site must be included in the calculation, and multiple-fit planes standing for different slopes in multiple directions are necessary.

In addition, the lack of energy-balance closure enables one to measure and estimate other terms in the conservation equation, i.e., horizontal and vertical advection. Estimating the non-turbulent components of CO_2 mass balance (horizontal and vertical advection) has become a major challenge for micrometeorologists (Lee 1998; Paw et al. 2000; Feigenwinter et al. 2004, 2008; Heinesch et al. 2007, 2008; Mammarella et al. 2007; Vickers and Mahrt 2006; Leuning et al. 2008). The two advective fluxes show different contributions in different experiments. Feigenwinter's calculation suggested that the two advective fluxes are opposite and seem to cancel each other at night (Feigenwinter et al. 2004), whereas Leuning thought the vertical and horizontal advection all contributed significantly to the mass balance (Leuning et al. 2008), and Mammarella's results suggested minor significance of horizontal advection (Mammarella et al. 2007). Estimation of vertical velocity is very important for calculating the vertical advection (VA). Several methods are used to calculate vertical velocity, including tilt-correction methods and the mass-conservation principle (Lee 1998; Paw et al. 2000; Feigenwinter et al. 2004; Vickers and Mahrt 2006; Leuning et al. 2008). Although much work has been done to improve energy balance, such as measuring all the major terms of the surface energy balance (Oncley et al. 2007; Vickers and Mahrt 2006; Feigenwinter et al. 2004), the problem is not solved well, so more exploration is needed. One issue of the effect of azimuth on the eddy-covariance flux and vertical velocity is often ignored; thus, error can be introduced because the property of heterogeneity is different for different wind directions for complex terrain. The present study will expand the PF method and focus on the effect of wind direction on the EC flux and calculation of vertical velocity.

Based on the expansion of PF methods in the present study, we compare the EC fluxes using both SPF and GPF methods. An expression of the vertical velocity is obtained, and estimations of the vertical velocity and vertical advection over the complex terrain are performed. The study is organized as follows: in Sect. 2, we briefly describe the theoretical process for expansion of the PF method and its application for vertical velocity over complex terrain.

Section 3 presents the site description and the experimental results. Finally, we provide a short summary.

2 Theory

Research has shown that ensemble-averaged slope flows are approximately parallel to the terrain slope close to the ground within the canopy layer (Sun 2007). A streamline coordinate system can be considered as the terrain-following coordinate system (Wilczak et al. 2001) and is often chosen for processing the measurements because it makes the data readily comparable to analytical theories, which are most easily cast in the streamline coordinate system. Flux measurements by the EC method can usually be performed with the wind sensors in the true horizontal and vertical planes, but the local terrain for EC systems is often not level. Therefore, a coordinate-system transformation needs to be done.

The PF method for a coordinate system transformation is briefly deduced and expanded here in a different way from that used by Wilczak et al. (2001).

The average of real vertical velocity over an extended period (e.g., a week or more) is close to zero. Therefore, it is assumed that the measured vertical velocity consists of two parts: one is the real vertical velocity from convection, synoptic-scale subsidence and local circulation (Lee 1998); the other is the tilt vertical velocity from the sonic anemometer and sloping terrain. We have:

$$\bar{w}_{\mathrm{m}} - b_0 = \bar{w}_{\mathrm{R}} + \bar{w}_{\mathrm{T}} \tag{1}$$

where $\bar{w}_{\mathrm{m}}$ is the temporal average of the vertical velocity measured over a 30-min interval with a sonic anemometer, and the bar means the mean value over a 30-min interval. $\bar{w}_{\mathrm{R}}$ and $\bar{w}_{\mathrm{T}}$ denote the real mean vertical velocity and the tilt vertical velocity, respectively. b_0 is a mean zero offset, possibly due to the electronic problems and flow perturbation in the measured vertical velocity. It is assumed that $\bar{w}_{\mathrm{R}}$ is random and that the average value of $\bar{w}_{\mathrm{R}}$ is zero over the long term, e.g., 1 or 2 weeks. This decomposition of $\bar{w}_m$ into $\bar{w}_{\mathrm{T}}$ and $\bar{w}_{\mathrm{R}}$ is essential and finally leads to the expression for the real vertical velocity in Eq. (10).

Thus, we obtain:

$$\sum_n \bar{w}_{\mathrm{R}} \to 0, \tag{2}$$

where n is the number of 30-min runs. $\bar{w}_{\mathrm{T}}$ is not a random function; it is a component of wind speed parallel to the terrain surface, which is a function of wind direction (hence topography) and instrument orientation attributed to the tower and anemometer. Thus, we now have:

$$\bar{w}_{\mathrm{T}} = b_1(\varphi)\bar{u}_{\mathrm{m}} + b_2(\varphi)\bar{v}_{\mathrm{m}} \tag{3}$$

where $b_1(\varphi)$ and $b_2(\varphi)$ are the wind direction φ-dependent coefficients. $\bar{u}_{\mathrm{m}}$ and $\bar{v}_{\mathrm{m}}$ are longitudinal and lateral velocity, respectively, measured by sonic anemometer. For a certain direction φ, the coefficients $b_1(\varphi)$ and $b_2(\varphi)$ tend to be the constants with long duration. Because $\bar{u}_{\mathrm{m}}$ and $\bar{v}_{\mathrm{m}}$ are often much larger than $\bar{w}_{\mathrm{m}}$, the biases in $\bar{u}_{\mathrm{m}}$ and $\bar{v}_{\mathrm{m}}$ of the same order as $b_0(\varphi)$ can be omitted. From Eqs. (1), (2) and (3), we obtain:

$$\sum_n \bar{w}_{\mathrm{R}} = \sum_n \left[\bar{w}_{\mathrm{m}} - b_0(\varphi) - b_1(\varphi)\bar{u}_{\mathrm{m}} - b_2(\varphi)\bar{v}_{\mathrm{m}}\right] \tag{4}$$

The forms of functions $b_0(\varphi)$, $b_1(\varphi)$ and $b_2(\varphi)$ are not known. Based on the characteristics of terrain topography, the terrain around the measurement site can be divided into sectors in which there are individual best-fit planes. For example, for simplicity, the complete 360° range can be divided into 12 sectors with a range of 30° each, and 12 planes can be fitted for each sector.

For each sector, the best-fit coefficients $b_0(\varphi)$, $b_1(\varphi)$ and $b_2(\varphi)$ can be obtained according to the PF approach of Wilczak et al. (2001). If $b_0(\varphi)$, $b_1(\varphi)$ and $b_2(\varphi)$ are not dependent on the wind direction φ and become constant, then this analysis is equivalent to the PF technique (Wilczak et al. 2001). Subsequently, EC flux can be obtained.

Based on previous analysis, after we obtain the coefficients $b_0(\varphi)$, $b_1(\varphi)$ and $b_2(\varphi)$, the real vertical velocity within 30 min and in each sector can be obtained as follows:

$$\bar{w}_{\mathrm{R}} = \bar{w}_{\mathrm{m}} - b_0(\varphi) - b_1(\varphi)\bar{u}_{\mathrm{m}} - b_2(\varphi)\bar{v}_{\mathrm{m}} \tag{5}$$

This equation is the real vertical velocity during a 30-min period. Equation (4) in Vickers and Mahrt (2006) is comparable to Eq. (5) here, but their calculation of vertical velocity ignored the effect of wind direction. Based on Eq. (5), a new expression will be deduced, and a clear meaning for the real vertical velocity can be derived.

For one sector, let $\bar{u}_{\mathrm{PFR}}$, $\bar{v}_{\mathrm{PFR}}$ and $\bar{w}_{\mathrm{PFR}}$ be the three wind components after the planar-fit rotation (Wilczak et al. 2001) is performed by coordinate-system transformation:

$$\bar{w}_{\mathrm{PFR}} = p_1 \cdot \bar{u}_{\mathrm{m}} + p_2 \cdot \bar{v}_{\mathrm{m}} + p_3 \cdot (\bar{w}_{\mathrm{m}} - b_0) \tag{6}$$

After Wilczak et al. (2001), the variables p_1, p_2 and p_3 can be obtained as follows:

$$p_1 = \frac{-b_1}{\sqrt{b_1^2 + b_2^2 + 1}}, p_2 = \frac{-b_2}{\sqrt{b_1^2 + b_2^2 + 1}} \text{ and } p_3 = \frac{1}{\sqrt{b_1^2 + b_2^2 + 1}} \tag{7}$$

Based on Eq. (5), (6) and (7), we have:

$$\bar{w}_{\mathrm{PFR}} = \left[\bar{w}_{\mathrm{m}} - (b_0 + b_1\bar{u}_{\mathrm{m}} + b_2\bar{v}_{\mathrm{m}})\right] / \sqrt{b_1^2 + b_2^2 + 1} \tag{8}$$

where:

$$\bar{w}_{PFR} = \bar{w}_R / \sqrt{b_1^2 + b_2^2 + 1} \qquad (9)$$

from which:

$$\bar{w}_R = \bar{w}_{PFR} \cdot \sqrt{b_1^2 + b_2^2 + 1} \qquad (10)$$

Equation (10) for vertical velocity is different from the others, which are based on the PF methods (Heinesch et al. 2007; Ono et al. 2008; Vickers and Mahrt 2006). After PF rotation, the z-axis in the new coordinate system is not orthogonal to horizontal direction, and the real vertical velocity is in the true vertical direction; thus, the direction of $\bar{w}_{PFR}$ is not that of the real vertical velocity. According to Wilczak et al. (2001), the cosine of the angle between the z-axis after the planar-fit rotation and the true vertical direction is $\frac{1}{\sqrt{b_1^2 + b_2^2 + 1}}$, and $\bar{w}_{PFR}$ is the component along the z-axis of $\bar{w}_R$ after the planar-fit rotation.

3 Applications to the Koflux data

3.1 Site and measurements

The data for this study were recorded on a 40 m high tower at the Gwangneung Forest site, Korea (37°45′25.37″N, 127°9′11.62″E) (Fig. 1). This site is part of the KoFlux program, which is dedicated to continuously measuring and studying water, carbon, and energy fluxes in key ecosystems of monsoon Asia. The site is dominated by an old natural forest of *Quercus* sp. and *Carpinus* sp. (80–200 years old), and the average canopy height is about 18 m. The tower is located near the headwater of the hilly deciduous forest catchment. The hillsides are dominated by slopes of 10°–20°, with a maximum slope of 51°. The whole catchment area is based on weathered gneiss and schist, with an eastern aspect. Typical soil depth is from 0.4 to 0.8 m, and the soil

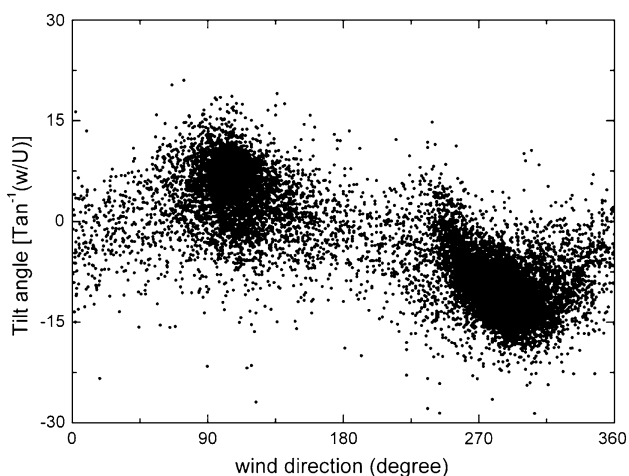**Fig. 1** Topography of the KoFlux site for Gwangneung Forest site

texture is mainly sandy loam. EC systems, an 8-level profile system and other instruments are present. The EC systems (CSAT3 and CR5000, Campbell Scientific.; LI7500, LiCor) were mounted at a height of 40 m. In addition, one H_2O/CO_2 concentration profile system (LI6262, LiCor; CR23X-TB and SDM-CD16AC, Campbell Scientific; vacuum pump, KNF Neuberger), similar to the one described by Feigenwinter et al. (2004), was installed on the tower. The measurement heights were 0.1, 1, 4, 8, 12, 20, 30, and 40 m. The sampling rates for the EC and profile systems were 10 and 4 Hz, respectively. The averaging time was 30 min. We selected 1 year of data, from 1 January 2006 to 31 December 2006. Data quality control was done using a serial process, including a spike check, range tests, tests of the diagnostic values from CSAT3 (Campbell Scientific Ltd. 2007) and LI7500 (LI-COR, Inc. 1999), planar-fit rotation (Wilczak et al. 2001), WPL calculation (Webb et al. 1980) and an integral turbulence-characteristics test (Foken et al. 2004). The data quality was determined at each step of the quality-control procedure and was denoted by four different quality flags (M for missing, B for bad, D for dubious and G for good data); only good data were used for this study. More information on the measurement system and data processing can be found in Kwon et al. (2007) and Hong et al. (2008).

We applied the PF rotation for several different sectors, considering the complex terrain and wind direction, and herein refer to this coordinate rotation scheme as a sector planar fit (SPF), whereas the corresponding scheme of ignoring wind direction as done by Wilczak et al. (2001) is called a general planar fit (GPF). All directions are divided into 12 sectors (with a range of 30° for each sector, 0°–30°, 30°–60° and so on) to consider the effect of rolling topography around the flux tower.

3.2 Results

3.2.1 Variance of tilt angles and PF coefficients with wind direction and duration

Figures 2 and 3 show the normalized vertical velocity variations with wind direction and their frequency distribution, respectively. Prevailing winds are southeasterly in daytime and northwesterly in nighttime, and vertical motion is related to this diurnal wind circulation. This change in wind direction indicates that the wind circulation at this site is controlled mainly by a mountain-valley circulation rather than by synoptic-scale flows. We note that a simple sinusoidal function is not appropriate to fit the apparent terrain slope $\left(\frac{\bar{w}}{\bar{u}}\right)$ against wind direction (Fig. 2); e.g., the classical GPF method should not be used to analyze the data from complex terrain. Such complex terrain slope is expected because the slope and aspect following the axis of the mountain-valley circulation are variable,

Fig. 2 The ratio of vertical (w) to horizontal wind speed (U) for tilt angle
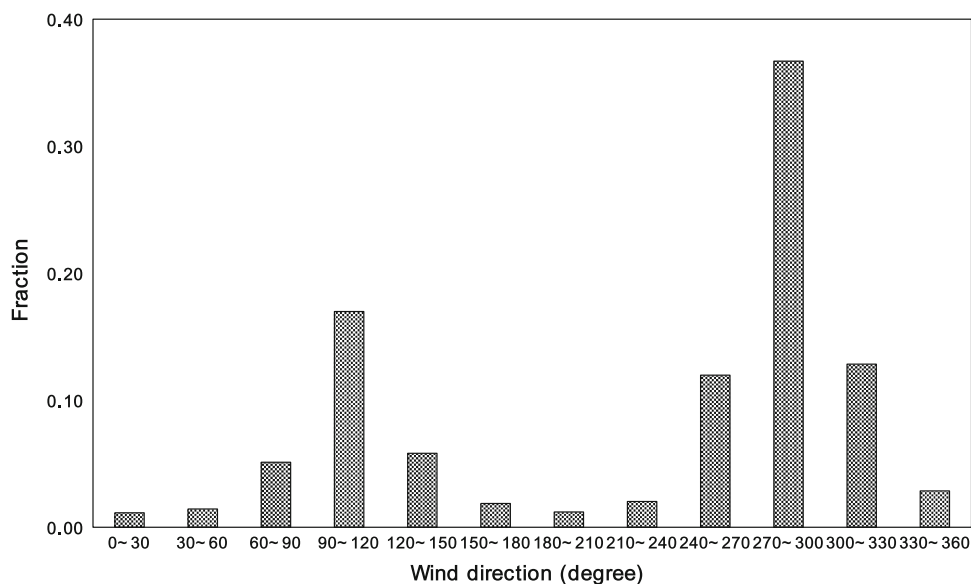
such that the tilt vertical velocity $\bar{w}_T$ should be considered as the azimuth function in Eq. (3).

Our analysis shows that the rotation angles of the coordinate frames obtained using the SPF scheme depart considerably from those obtained by the GPF scheme. Such a significant difference is expected if we consider the complex topography around the tower, again emphasizing that an appropriate PF rotation should be applied with different wind sectors. In the case of southeasterly winds, the difference in the rotation angle between the SPF and GPF methods was smaller than in other directions (Fig. 4). In Fig. 4, the pitch angle α and roll angle β, following Eq. 2 and Fig. 1 in Wilczak et al. (2001), are calculated as:

$$\alpha = \sin^{-1}\left(\frac{-b_1}{\sqrt{b_1^2+b_2^2+1}}\right), \text{ and } \beta = \sin^{-1}\left(\frac{-b_2}{\sqrt{b_2^2+1}}\right) \text{ where } \alpha$$

and β denote rotation angle, further representing the scale of terrain slope.
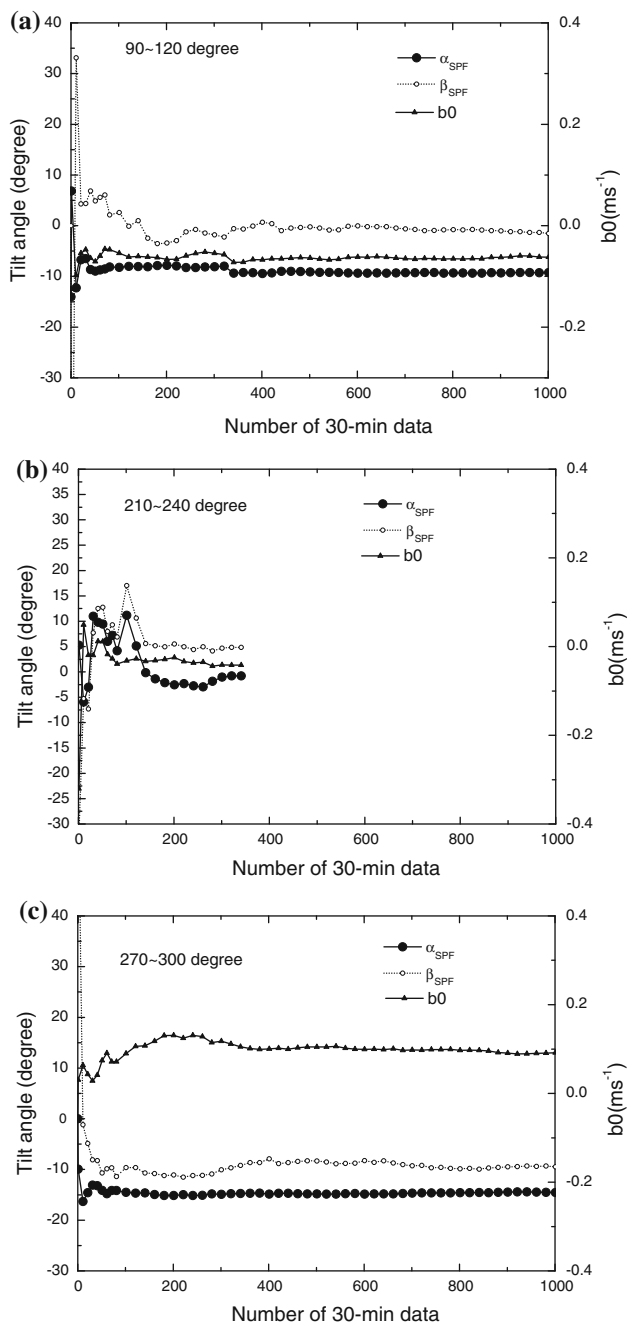
However, the tilt angle in the northward direction was larger than in the southeastward direction. We believe that the changes of slope and aspect across the forest catchment directly influence the tilt plane constructed by the GPF scheme because typical flux footprints are >1 km at night (Baldocchi 1997; Kim et al. 2006). The zero offset of w (b_0) from the PF rotation was about -0.05 m s^{-1} in daytime, when southeasterly flows were dominant. However, this offset of w was around $+0.1$ m s^{-1} at night. This result indicates that the offset of w computed from the PF rotation is a function of the instrument's electronic bias as well as the flow conditions. This result also has important physical implications in the 2- and 3-dimensional flow characteristics that impact the estimation of the net eco-system production at a non-ideal site such as the Gwang-neung site (Lee and Hu 2002). The positive (negative)

Fig. 4 The variation of the zero offset b_0, the pitch (α) and roll (β) angles for Gwangneung Forest site. The subscripts 'GPF' and 'SPF' denote GPF and SPF schemes, respectively

Fig. 3 Wind direction distribution with the bin of 30° sector

non-zero offset observed in this study could results in overestimation (underestimation) of the net ecosystem production during nighttime (daytime).

To obtain stable PF coefficients, sufficient 30-min data are needed. Figure 5 indicates that the PF coefficients and pitch and roll angles vary with the quantity of data. Here, only three sectors are used as examples (Fig. 5). The sectors 90°–120° and 270°–300° are two prevailing wind directions,

and the sector 210°–240° is only one of the non-prevailing wind directions for comparison with other sectors.

We note that the pitch and roll angles quickly converge to a constant value after 200 half-hourly data sets have been integrated. These correspond to about 1–2 weeks of data collected for each prevailing wind direction (e.g., 90°–120°, 270°–300°), likely reflecting the synoptic-scale influences on the PF rotation (Fig. 5a, b). We note that the roll angle for the 90°–120° sectors shows a gradual change up to 600 half-hourly data sets to get a stable value, indicating variability in the angles' decreases with increasing sample size. For other sectors of less frequent wind directions, this stabilization would take much longer (i.e., weeks to months) (Fig. 5c).

3.2.2 Comparison of EC flux by GPF with SPF schemes

When the planar-fit technique is applied to calculate flux, the data from all wind directions are often used to determine a stable reference frame (Lee et al. 2004). However, based on the analysis above, the coefficients of b_0 and the tilt angle strongly depend on wind direction. Therefore, in such complex terrain as Gwangneung Forest, when the planar-fit coefficients are calculated from comprehensive direction data, the data of the dominant direction give the largest contribution. This finding means that GPF coefficients represent the dominant direction. If GPF coefficients are used for a sector that is not the dominant direction, then a large error for flux calculation may occur.
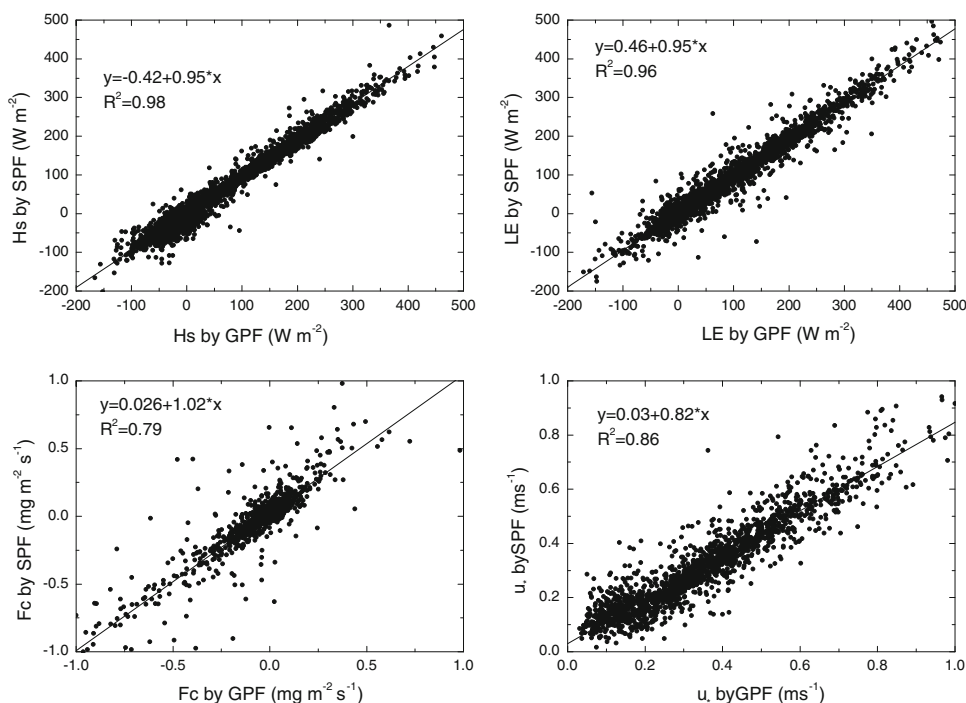
First, we used the GPF scheme to calculate the coefficients b_0, b_1 and b_2 as well as momentum, sensible heat, latent heat and CO_2 fluxes. Second, we used the SPF scheme to calculate the coefficients and fluxes. Then, the two sets of fluxes were compared. Here, we take the data with the direction within the sector (240°–270°) as an example and calculate the coefficients and then the fluxes. There are over 3,000 runs within this sector. Table 1 gives the coefficients and tilt angles calculated from the two schemes. Both the coefficients and tilt angles between the two schemes show substantial difference.

Figure 6 compares the EC terms of latent heat flux (LE), sensible heat flux (Hs), CO_2 flux (Fc) and friction velocity (u*) by GPF and SPF schemes. The abscissa is the flux by the GPF scheme, and the ordinate is the flux by the SPF scheme. The regression lines are convenient for comparing the two results.

Fig. 5 The tilt angles and vertical velocity offsets b_0 for Gwangneung Forest site. **a** is within the 90°–120° sector, and **b** is within the 210°–240° sector, and **c** is within the 270°–300° sector

Table 1 The coefficients and tilt angle

Data set	b_0 (m/s)	b_1 (unitless)	b_2 (unitless)	Pitch angle α	Roll angle β
GPF	−0.054	0.177	−0.074	10.0	4.2
SPF	−0.0015	0.236	−0.276	12.8	15.0

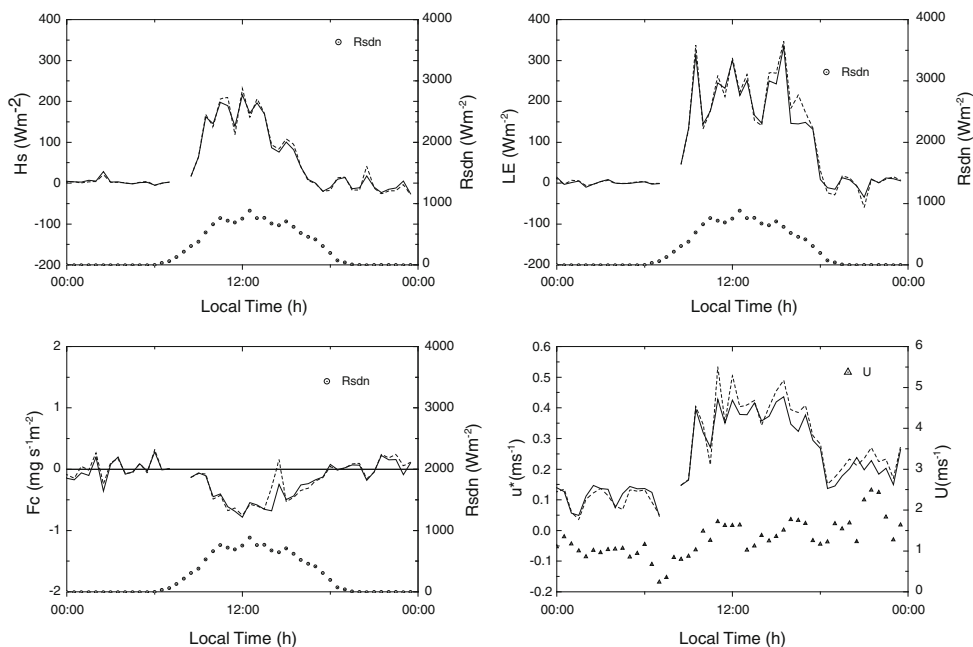Fig. 6 Comparison of LE, Hs, Fc and $u*$ by GPF and SPF within 240°–270°

The slopes of comparisons of Hs, LE, Fc, and $u*$ are 0.95, 0.95, 1.02, and 0.82, respectively; the relative errors vary by 2–18%. There are small differences between scalar fluxes and a slightly larger difference between moment fluxes. The coefficients of determination for Hs, LE, Fc, and $u*$ are 0.98, 0.96, 0.79, and 0.86, respectively. The large coefficients apparently indicate that the correlation is high, but the fact that the slopes of the regression lines are not equal to one hints at a systematic error. The error may be due to the different methods of coordinate rotations.

Despite the fact that the SPF and GPF methods did not show much difference in surface fluxes at the site, the SPF method yields less variation in flux values than the GPF (Fig. 7). Caution must be exercised in interpreting individual surface-flux measurements. For example, under sunny conditions, the diurnal patterns and magnitudes of

Fig. 7 EC part of Hs, LE and Fc and $u*$ on 12 August 2006, straight line for SPF and dot curve for GPF

Hs, LE and $u*$ from the two rotations show no significant differences. However, fluxes Fc and $u*$ from the SPF rotation produced more plausible magnitudes and patterns, whereas the results from the GPF were unrealistic; i.e., $Fc = 0.15$ mg s^{-1} m^{-2} between 1,400 and 1,430 local time on 12 August 2006, when $R_{sdn} = 700$ W m^{-2} and CO_2 fluxes at the adjacent moment were negative.

Careful inspection of the comparison in Fig. 6 reveals that some individual data points show large deviations for CO_2 and momentum (up to 50%). For our experimental site, the differences in pitch angle α and roll angle β are not small. Taking the 240°–270° sector as an example, the difference of pitch angle α between GPF and SPF is 2.8° (Fig. 4), and the difference of the roll angle β between GPF and SPF is 11.2°. Therefore, the differences in the rotation angles are substantial, and the slope of the regression line does not reach 1. For momentum, the procedure of calculation is different from that for the scale fluxes. As for the relatively large bias in the CO_2 and momentum flux, we analyze them by the following: Here, the relatively large bias means deviation from the regression line, so deviation can be calculated as:

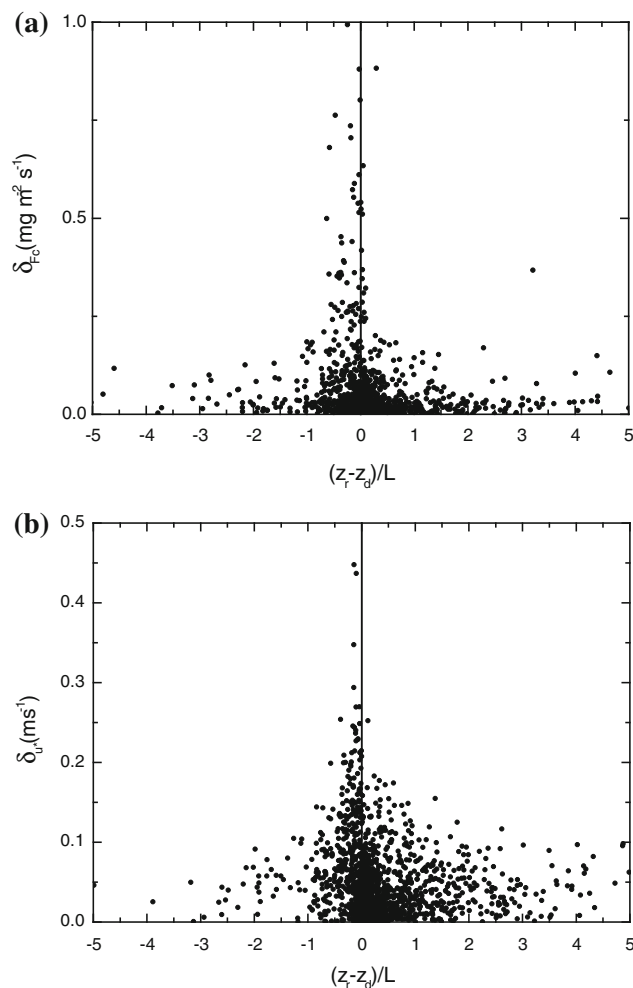$$\delta_{Fc} = |Fc_{SPF} - 0.026 - 1.02 \times Fc_{GPF}| \qquad (11)$$

Fc_{SPF} denotes CO_2 flux by the SPF method and Fc_{GPF} by the GPF method.

To analyze the relatively large bias in CO_2 and momentum flux, we show the relation of deviation against stability [$(z_r - z_d)/L$, where z_r is the measurement height, z_d is canopy height and L is Monin–Obukhov length], shown in Fig. 8a. Figure 8a shows that the deviation is large under near-neutral to mildly unstable condition. The deviations of the moment flux have the same characteristic with stability as the CO_2 flux (Fig. 8b).

3.2.3 Characteristics of vertical velocities and vertical advection term of flux

Based on the analysis above, the vertical velocity can be calculated according to the Eq. (10). Following the former consideration, the PF coefficients b_0, b_1 and b_2 within the 12 sectors are used for calculating the real vertical velocities $\bar{w}_r$. Figure 9a gives the distribution of vertical velocities over the Guangneng Forest. There are three vertical velocity curves given by the temporal average of the vertical velocity measured over a 30-min interval with a sonic anemometer and calculated using the GPF and SPF methods. From Fig. 9a, the SPF results are closer to the normal distribution than the others are.

Figure 9b gives the variations of the vertical velocities during a sunny day: 12 August 2006. In Fig. 9b, the dashed line is obtained by the GPF scheme, and the solid line is obtained with 12 different sectors by the SPF scheme.
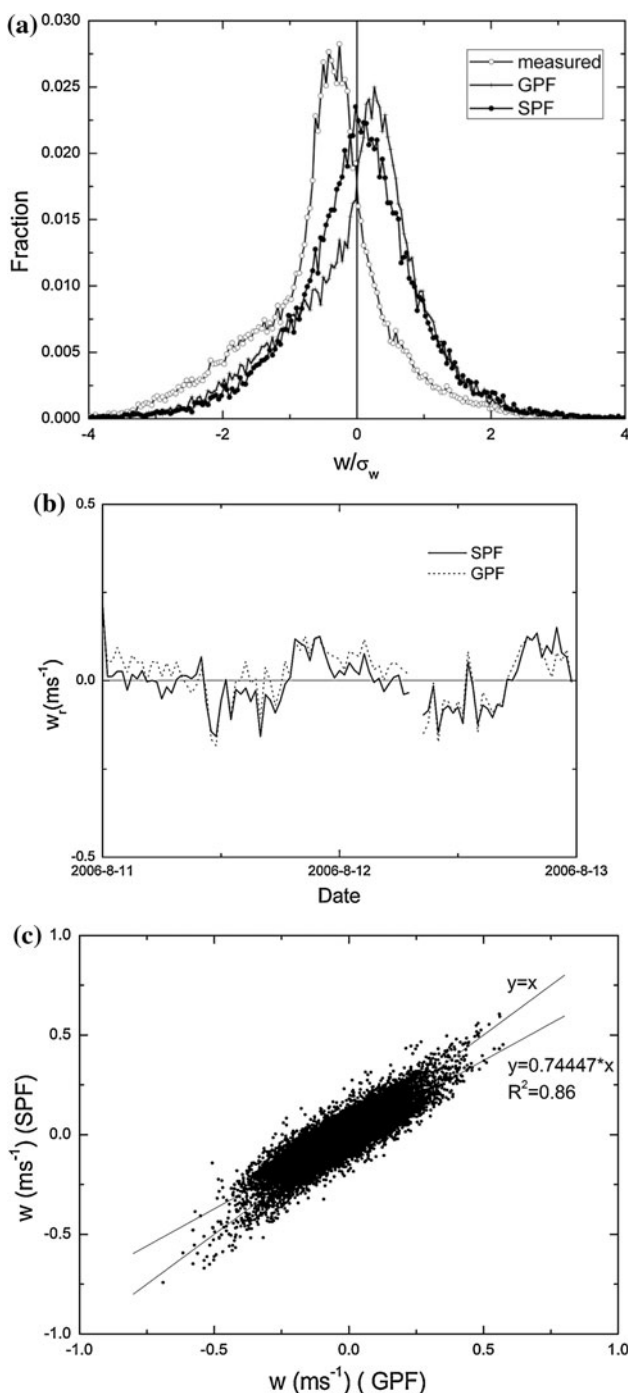

Fig. 8 Relation of deviation of CO_2 flux against stability [$(z_r - z_d)/L$, z_r is the measurement height, z_d is canopy height, L is Monin–Obukhov length]

The two schemes show similar and obvious diurnal variations. During daytime, the real vertical velocity is negative, and during nighttime, it is positive. These results may be due to the local circulation at the measurement position. There are some differences between the two lines, especially under weak vertical velocities. From sunset to midnight, vertical velocities by SPF are weaker than by GPF. This difference can also be seen in Fig. 9c, which shows a comparison of vertical velocities between the GPF and SPF schemes. Two lines are shown in Fig. 9c; one is the fitting line and the other is the one-to-one line. Based on the Fig. 9c, the vertical velocity values derived by the SPF scheme become approximately 25% lower than values from GPF, especially for weak vertical velocities, e.g., less than about 0.2 m/s.

The smaller variation in mean vertical wind speed by the SPF method, (Fig. 9b), is possibly due to the rotation angle of the SPF method from a small sector (namely a 30° sector) instead of a 360° sector.

Fig. 9 Comparisons of the vertical velocity between two methods of GPF and SPF. **a** is the distribution with the bin of 0.04 ms^{-1} before and after PFR and **b** diurnal variation of vertical velocity 12 August 2006, the *solid line* by SPF and *dashed curve* by GPF. **c** is comparison of vertical between the different methods

The average value of $\bar{w}_r$ by SPF is zero, and the individual values have a normal distribution. The average value of $\bar{w}_r$ given by GPF, however, is not zero, so the regression line is not equal to 1. From the vertical wind

distribution (Fig. 9a), the difference between GPF and SPF is mainly due to the distribution of weak vertical velocities.

Following Lee (1998), the vertical advection term is:

$$\int_0^{z_r} \bar{w}\frac{\partial \bar{c}}{\partial z}\mathrm{d}z = \bar{w}_{z_r}\bar{c}_{z_r} - \bar{w}_{z_r} \cdot \langle \bar{c}\rangle \tag{12}$$

$\bar{w}_{z_r}$ is the real mean vertical velocity at the measurement height z_r, which needs to be calculated, and the bracket $\langle\rangle$ is the spatial average concentration between the ground and this height.

Based on the Eq. (12), the data for 1 day, 12 August 2006, from 8-level profiles and EC systems were used to calculate the vertical advection terms of sensible heat flux, latent heat flux and CO_2 flux (Fig. 10). Of the two curves in Fig. 10, the dashed curve signifies the GPF scheme, and the solid curve signifies the SPF scheme. These show similar trends in general but are occasionally very different.

The vertical advection of sensible heat flux has large positive values during nighttime and has little fluctuation during other times; the calculated results by GPF are larger than by SPF from midnight to morning because of the difference of vertical velocities by the two methods. For water vapor and CO_2, the vertical advection fluxes have a large positive value during the afternoon and a large negative value during the night.

The smaller variation in mean vertical advection by the SPF method is caused by the same factors that affect vertical velocity.
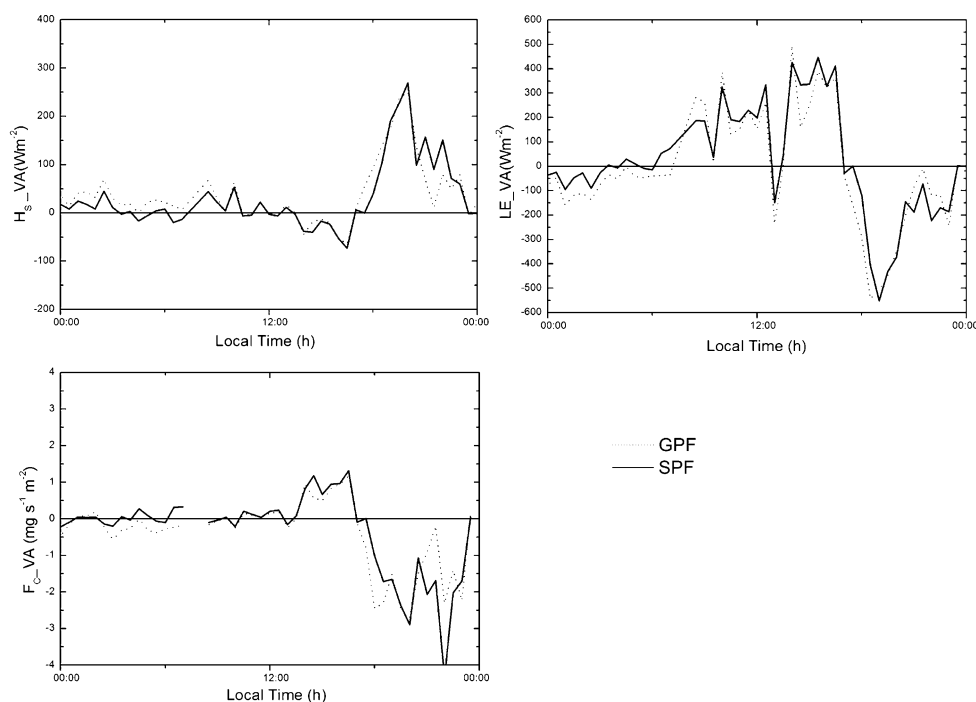
4 Summary and concluding remarks

In this paper, we expanded the PF method and applied it to calculate EC and VA fluxes and vertical velocity. Because of the complexity of terrain, wind direction must be considered in the PF method. Moreover, Koflux data were used to calculate the PF coefficients, which show the difference between using the GPF and SPF methods.

We applied the expanded PF method to half-hourly data by sectors of 30°. Two hundred 30-min data sets are enough for stable PF coefficients over a hilly terrain such as the Gwangneung supersite, but the duration and number of samples depend on wind direction. The offset of the mean vertical wind speed was about |0.05| m s^{-1} with the opposite sign between daytime and nighttime. Turbulent fluxes can be biased because of the apparent tilt angle caused by such a mean offset. The 30°-sector range was selected for simplicity. As for another complex site, a selection of a different range may be made.

Based on the comparison of the EC flux by GPF and SPF, scalar flux showed better agreement than the friction

Fig. 10 Vertical advection part of Hs_VA, LE_VA and Fc_VA on 12th August in 2006, straight line using SPF and dot curve using GPF

velocity. Friction velocity is an important scaling variable in the atmospheric boundary layer and a critical parameter for the nighttime data filtering (i.e., u^* correction) (Foken et al. 2004).

This paper provides an explanation of measurement results for vertical wind and real vertical velocity. It is assumed that the real vertical velocities over the long term have a zero mean. An expression for the real vertical velocity is obtained. Over complex terrain such as the Gwangneung Forest, the wind direction must be considered when the real vertical velocity is calculated. After the wind direction is considered, the distribution of the real vertical velocities is close to normal, and the values of the real vertical velocities have a large difference from the GPF velocities, where the wind direction is disregarded, especially under weak vertical velocity conditions.

The SPF method for both EC-term and VA-term flux yields less variation than the GPF method.

In relation to such biases between the GPF and SPF methods, further scrutiny of their relationship with horizontal advection is currently in progress.

References

Baldocchi D (1997) Flux footprints within and over forest canopies. Bound Layer Meteorol 85(2):273–292

Baldocchi DD (2003) Assessing the eddy covariance technique for evaluating carbon dioxide exchange rates of ecosystems: past, present and future. Glob Chang Biol 9(4):479–492

Baldocchi DD, Falge E, Gu L, Olson R, Hollinger D, Running S, Anthoni P, Bernhofer Ch, Davis K, Fuentes J, Goldstein A, Katul G, Law B, Lee X, Malhi Y, Meyers T, Munger W, Oechel W, Paw UKT, Pilegaard K, Schmid HP, Valentini R, Verma S, Vesala T, Wilson K, Wofsyn S (2001) FLUXNET: a new tool to study the temporal and spatial variability of ecosystem-scale carbon dioxide, water vapor, and energy flux densities. Bull Am Meteorol Soc 82:2415–2434

Campbell Scientific Ltd. (2007) CSAT3 Three Dimensional Sonic Anemometer User's Guide, 70 pp

Feigenwinter C, Bernhofer C, Vogt R (2004) The influence of advection on the short term CO_2 budget in and above a forest canopy. Bound Layer Meteor 113:201–224

Feigenwinter C, Bernhofer C et al (2008) Comparison of horizontal and vertical advective CO_2 fluxes at three forest sites. Agric For Meteor 148(1):12–24

Finnigan JJ (1999) A comment on the paper by Lee (1998): on micrometeorological observations of surface-air exchange over tall vegetation. Agric For Meteorol 97:55–64

Foken T, Gockede M, Mauder M, Mahrt L, Amiro BD, Munger JW (2004) Post-field data quality control. In: Lee X, Massman WJ, Law BE (eds) Handbook of micrometeorology. A guide for surface flux measurements. Kluwer, Dordrecht, pp 181–208

Heinesch B, Yernaux M et al (2007) Some methodological questions concerning advection measurements: a case study. Bound Layer Meteorol 122(2):457–478

Heinesch B, Yernaux Y et al (2008) Dependence of CO_2 advection patterns on wind direction on a gentle forested slope. Biogeosciences 5(3):657–668

Hong J, Kim J, Lee D, Lim JH (2008) Estimation of the storage and advection effects on H2O and CO_2 exchanges in a hilly KoFlux forest catchment. Water Resour Res 44: W01426. doi:10.1029/2007WR006408

LI-COR, Inc (1999) LI-7500 CO_2/H_2O Analyzer Instruction Manual, 133 pp

Kaimal JC, Finnigan JJ (1994) AtmosphericBoundary Layer Flows: Their Structure and Measurement. Oxford University Press, New York, p 289

Kim J, Guo Q et al (2006) Upscaling fluxes from tower to landscape: overlaying flux footprints on high-resolution (IKONOS) images of vegetation cover. Agric For Meteorol 136(3–4):132–146

Kwon H, Park SB, Kang M, Yoo J, Yuan RM, Kim J (2007) Quality control and assurance of Eddy covariance data at the two KoFlux sites. Korean J Agric For Meteorol 9:260–267

Lee X (1998) On micrometeorological observations of surface-air exchange over tall vegetation. Agric For Meteorol 91:39–49

Lee X, Hu X (2002) Forest-air fluxes of carbon, water and energy over non-flat terrain. Bound Layer Meteorol 103:277–301

Lee X, Massman W, Law B (2004) Handbook of micro-meteorology: a guide for surface flux measurement and analysis. Kluwer Academic Publishers, Dordrecht, p 250

Leuning R, Zegelin SJ et al (2008) Measurement of horizontal and vertical advectlion of CO_2 within a forest canopy. Agric For Meteorol 148:1777–1797

Mammarella I, Kolari P et al (2007) Determining the contribution of vertical advection to the net ecosystem exchange at Hyytiala forest, Finland. Tellus B Chem Phys Meteorol 59(5):900–909

Mauder M, Oncley SP et al (2007) The energy balance experiment EBEX-2000. Part II: Intercomparison of eddy-covariance sensors and post-field data processing methods. Bound Layer Meteorol 123(1):29–54

Oncley SP, Foken T et al (2007) The energy balance experiment EBEX-2000. Part I: Overview and energy balance. Bound Layer Meteorol 123(1):1–28

Ono K, Mano M, Miyata A, Inoue Y (2008) Applicability of the planar fit technique in estimating surface fluxes over flat terrain using eddy covariance. J Agric Meteorol 64:121–130

Paw UKT, Baldocchi DD, Meyers TP, Wilson KB (2000) Correction of eddy-covariance measurements incorporating both advective effects and density fluxes. Bound Layer Meteorol 97:487–511

Sun JL (2007) Tilt corrections over complex terrain and their implication for CO_2 transport. Bound Layer Meteorol 124(2):143–159

Tanner CB, Thurtell GW (1969) Anemoclinometer measurements of Reynolds stress and heat transport in the atmospheric surface layer, Research and Development Tech. Report ECOM 66–G22-F to the US Army Electronics Command, Dept. Soil Science. University of Wisconsin, Madison

Vickers D, Mahrt L (2006) Contrasting mean vertical motion from tilt correction methods and mass continuity. Agric For Meteorol 138(1–4):93–103

Webb EK, Pearman GI, Leuning R (1980) Correction of the flux measurements for density effects due to heat and water vapour transfer. Quart J Roy Meteorol Soc 106:85–100

Wilczak JM, Oncley SP, Stage S (2001) Sonic anemometer tilt correction algorithms. Bound Layer Meteorol 99:127–150

Yu GR, Wen XF, Tanner BD, Sun XM, Lee X, Chen JY (2006) Overview of ChinaFLUX and evaluation of its eddy covariance measurement. Agric For Meteorol 137:125–137